TOPICAL REVIEW — Magnetism, magnetic materials, and interdisciplinary research

Exchange bias in ferromagnet/antiferromagnet bilayers*

Shi Zhong(时 钟)[a], Du Jun(杜 军)[b], and Zhou Shi-Ming(周仕明)[a]†

[a] Shanghai Key Laboratory of Special Artificial Microstructure Materials & Technology and School of Physics Science and Engineering, Tongji University, Shanghai 200092, China

[b] Department of Physics, Nanjing University, Nanjing 210093, China

(Received 17 September 2013; revised manuscript received 25 November 2013; published online 20 December 2013)

Since the exchange bias (EB) effect was discovered in the Co/CoO core-shell nanoparticles, it has been extensively studied in various ferromagnet (FM)/antiferromagnet (AFM) bilayers due to its crucial role in spintronics devices. In this article, we review the investigation of the EB in our research group. First, we outline basic features of the EB, including the effects of the constituent layer thickness, the microstructure and magnetization of the FM layers, and we also discuss asymmetric magnetization reversal process in wedged-FM/AFM bilayers. Secondly, we discuss the mechanisms of the positive EB and the perpendicular EB. Thirdly, we demonstrate the hysteretic behavior of the angular dependence of the EB and analyze the EB training effect. Finally, we discuss the roles of the rotatable anisotropy in the two phenomena.

Keywords: exchange bias, ferromagnet, antiferromagnet, bilayers

PACS: 75.30.Et, 75.30.Gw, 75.60.Jk **DOI:** 10.1088/1674-1056/23/2/027503

1. Introduction

In 1956, Meiklejohn and Bean[1] found that, for the Co/CoO core/shell nanoparticles, the centre of the hysteresis loop was located at −1.0 kOe (1 Oe = 79.5775 A/m) and the coercivity H_C was 2.2 kOe after the sample field cooled. However, after zero magnetic cooling, the hysteresis loop was centred at the zero magnetic field with H_C of about 1.0 kOe, as shown in Fig. 1. The phenomenon of both the shift of the hysteresis loops along the horizontal axis and the H_C enhancement is referred to as the exchange bias (EB). At the same time, non-vanishing rotational hysteresis was observed, even for the external magnetic field larger than the anisotropic field. Similar phenomena were also observed in Fe–FeO particles,[2] disordered Ni–Mn,[3] disordered and ordered Fe–Al alloys,[4] etc. The shift of the hysteresis loop and the non-zero rotational hysteresis at high magnetic fields can be used as a fingerprint of the EB.[5]

The first observation of the exchange bias in ferromagnt/antiferromagnet (FM/AFM) bilayers was reported in CoO/Co ones.[6] The EB phenomena in FM/AFM bilayers have received renewed attention since the discovery of the giant magnetoresistance effect in magnetic multilayers.[7–12] For practical applications of the giant magnetoresistance effect, the spin valve structure is designed. As the central part, FM/AFM bilayers play a crucial role and one of two FM layers is pinned by neighbouring an AFM layer so that the free FM layer can be reversed within a very small external magnetic field.[8] At present, the FM/AFM bilayer structure is widely used in various spintronics devices. Ideally, a large exchange field H_E, small H_C, and high thermal stability are required. Therefore, most of studies in this community have been made to optimize the performance of the EB by using various FM and AFM layers.

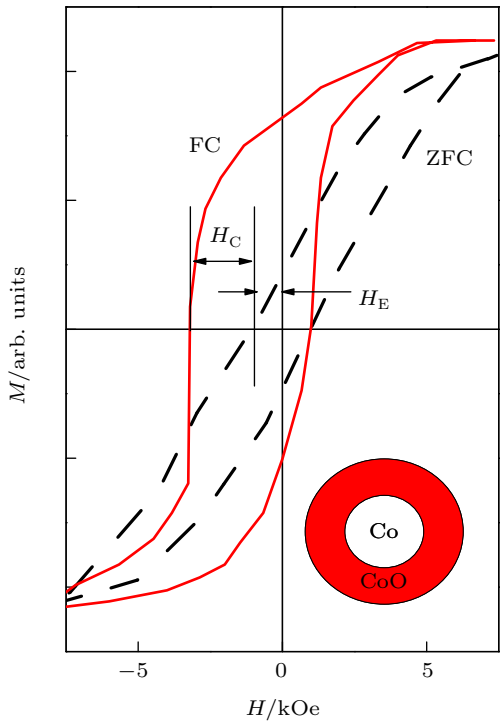


Fig. 1. (color online) Hysteresis loops at low temperatures of Co/CoO core/shell particles after field cooling (solid line) and zero field cooling (dashed line).[1]

Since the EB is caused by the exchange interaction between FM and AFM atomic magnetic moments at the inter-

*Project supported by the National Natural Science Foundation of China (Grant Nos. 10174014, 60271013, 60490292, 10574026, 50625102, 50871030, 10974032, 51171129, and 51201114) and the National Basic Research Program of China (Grant Nos. 2009CB929201 and 2010CB923401).

†Corresponding author. E-mail: shiming@tongji.edu.cn

© 2014 Chinese Physical Society and IOP Publishing Ltd

face, it is significant to reveal the physics behind the phenomena. Owing to its interfacial nature, H_E is expected to be proportional to the inverse FM layer thickness ($1/t_{FM}$) and H_C to become smaller for large t_{FM} at a fixed AFM layer thickness t_{AFM}.[6] In contrast, the EB depends on t_{AFM} in a more complex way. Since the EB is generally established at temperatures below the Neél temperature T_N of the AFM layers, it is strongly related to both the ordering degree of the AFM spins and the sampling temperature (T).[9] As the interfacial exchange coupling energy strongly depends on the spin structure of the FM and AFM layers at the interface, either compensated or uncompensated, the EB depends on crystalline orientations of the constituent layers.

In this article, we will primarily discuss our investigations of the EB phenomena over the past decade. Here, we mainly focus on the case of $T_C > T_N$ with T_C =the Curie temperature of FM layers.[13,14] In the second part, we will outline the basic features of the EB in various FM/AFM bilayers, including the effects of the thickness of constituent layers, the microstructure of the FM layers, and the FM magnetization. In the following third part, the positive EB in GdFe–NiCoO will be analyzed. Then, we will describe the perpendicular EB in NiFe/CoO multilayer. In the fifth part, the hysteresis behavior of the angular dependence of the EB (ADEB) will be introduced. In the last part, we will demonstrate the EB training effect and analyze the mechanisms of the pinning direction (PD) rotation and rotatable anisotropy in both the EB training effect and the hysteretic behavior of the ADEB.

2. Basic features of EB

2.1. Effects of AFM layer thickness

All the samples discussed in this article were fabricated by high vacuum multi-source magnetron sputtering. Large samples of the Si substrate (1.5 cm × 5 cm)/Cu (30 nm)/$Fe_{50}Mn_{50}$(= FeMn) (30 nm)/$Ni_{81}Fe_{19}$(= Py) multilayers were deposited from alloy targets of Py and $Fe_{50}Mn_{50}$. Here, the Py layer took a wedge shape from 4.0 nm to 30.0 nm across a distance of 5 cm of the substrate.[15,16] The Cu underlayer was used to stimulate the growth of fcc FeMn with (111) texture. Each location on the specimen along the wedge direction therefore corresponded to a specific Py thickness. During deposition, a magnetic field of about 200 Oe was applied in the film plane and perpendicular to the wedge direction. After deposition, the sample was heated to above T_N = 500 K of FeMn and cooled to room temperature in a magnetic field of 10 kOe, applied in the film plane and in the direction perpendicular to the wedge. Meanwhile, the Py/FeMn bilayers with varying t_{AFM} were also fabricated. Finally, the specimens of substrate(Si)/$Cr_{82}Al_{18}$(= CrAl)(t_{AFM})/Py (8 nm) with a wedged CrAl layer and Si/CrAl(53 nm)/Py(t_{FM}) with a wedged Py layer,[17] were deposited from Py-alloyed target and an Al target with small Cr pieces on it, before capping with a 30-nm thick Cu top layer. In the early 1960s, Kouvel and Kasper[18] discovered that disordered fcc-Fe_xMn_{1-x} alloys were found to have a long range antiferromagnetic order. Non-collinear spin structure was experimentally determined by a neutron scattering technique. The Fe spins are assumed to be ferromagnetically coupled while the neighbouring Mn–Mn and Mn–Fe spins are antiferromagnetically coupled. When the coupling strengths of the Fe–Fe, Mn–Fe, and Mn–Mn pairs are comparable, the neighbouring Mn spins will be aligned noncollinearly.[19] At the same time, atomic magnetic moments of Fe and Mn were determined to be 1.0 ± 0.2 μ_B and 1.2 ± 0.2 μ_B, respectively.[20] The CrAl alloy with 18 at.% Al is an AFM with Neél temperature of 500 °C–600 °C[21] and the spin structure of a spin density wave is formed with the atomic magnetic moment of about 1.0 μ_B.[22]

Dependence of the EB on the thickness of constituent layers has been studied extensively.[23–28] For the present Py/FeMn bilayers, H_E equals zero for $t_{AFM} < 3.0$ nm. It emerges only for $t_{AFM} > 3.0$ nm and then sharply increases to a maximal value with the increasing of t_{AFM}. H_C sharply increases at small t_{AFM} and reaches a maximum at $t_{AFM} = 10$ nm where H_E changes sharply. After that, H_C gradually decreases. The critical t_{AFM} value is close to the observed results by other research groups.[23,29–33] As shown in Fig. 2(b), for Py/CrAl bilayers, the onset thickness of the EB is equal to 25 nm, about one order in magnitude larger than that of 3.0 nm for Py/FeMn bilayers.[17] Apparently, the onset thickness of the EB depends on the AFM material. It is generally believed that the EB can be established for $t_{AFM}K_{AFM} > \Delta\sigma$ ($\Delta\sigma$ = interfacial exchange coupling energy) because, for $t_{AFM} > \Delta\sigma/K_{AFM}$, the AFM spins are thermally stable during the FM magnetization reversal process, leading to nonzero H_E. Otherwise, for $t_{AFM} < \Delta\sigma/K_{AFM}$, the AFM spins are in an unstable state, leading to zero H_E. Near the critical t_{AFM}, most of the AFM grains experience irreversible rotation during the FM magnetization reversal process and H_C is sharply enhanced. The H_E and H_C decrease for large t_{AFM} may indicate the degeneration of the microstructure or biquadratic coupling between FM and AFM layers.[34] The non-monotonic variation of the H_E with t_{AFM} was also explained as a result of the competing contributions between the net magnetization and the thermal stability of the AFM layers.[35] With the data of the $\Delta\sigma$ and the critical t_{AFM}, the uniaxial anisotropy constant K_{AFM} at room temperature can be evaluated and is 1.9×10^3 erg/cm^3 (1 erg = 10^{-7} J) and 1.0×10^5 erg/cm^3 for CrAl and FeMn layers, respectively. For FeMn layers, the uniaxial anisotropy is about 4 orders smaller than the theoretically predicted value of the cubic anisotropy constant (10^9 erg/cm^3).[36] It is also noted that for Py/CrAl bilayers the value of H_C is larger than

that of H_E and *vice versa* for Py/FeMn bilayers, demonstrating different performances of FeMn and CrAl allys in terms of EB.

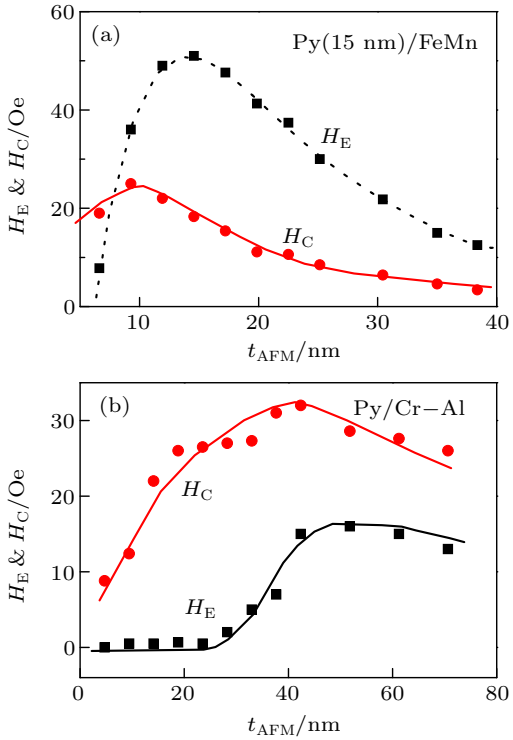


Fig. 2. (color online) Dependence of H_E and H_C at room temperature on t_{AFM} for Py/FeMn (a) and Py/CrAl (b) bilayers.[15,17]

2.2. Effects of FM layer thickness and asymmetry of a magnetization reversal process

Figure 3 shows that for Py/FeMn and Py/CrAl bilayers, H_E and H_C decrease with the increasing of t_{FM}. For the two series of bilayers, H_E demonstrates linear dependence on the inverse FM layer thickness $1/t_{FM}$. With $\Delta\sigma = H_E t_{FM} M_{FM}$ and the data of both the FM magnetization and the slope of the H_E versus $1/t_{FM}$ curve, the exchange coupling energy $\Delta\sigma$ is estimated to be 4.7×10^{-3} erg/cm^2 and 0.053 erg/cm^2 for Py/CrAl and Py/FeMn bilayers,[16,17] respectively. When $1/t_{FM}$ approaches zero, H_E is often close to a nonzero finite value due to two possible reasons. During the FM magnetization reversal process, a planar domain wall might occur in a thick FM layer, leading to nonzero intercept of the H_E versus $1/t_{FM}$ curve. Of course, this phenomenon might also be caused by either the measurement error of t_{FM} or the discontinuous morphology of the ultrathin FM layer. Noticeably, H_C changes as a linear function of $1/t_{FM}$ for Py/FeMn bilayer, whereas it obeys a linear dependence on $1/t_{FM}^{3/2}$ for Py/CrAl bilayer. Similar phenomena were also observed in Py/CoO bilayer and explained in terms of the random field model.[37,38]

The asymmetric hysteresis loops are often believed to be another fingerprint of the EB in FM/AFM bilayers. The asymmetric magnetization reversal process is attributed to the competition between the unidirectional and the uniaxial anisotropies in the frame of the coherent rotational mode.[39] As shown in Fig. 4, the switching fields H_{sw1} and H_{sw2} for wedged-Py/FeMn bilayers change with the sampling location, i.e. the FM thickness t_{FM}.[16] Accordingly, due to the wedged shape of the FM layer, a single domain wall is expected during the FM magnetization reversal process in each small specimen, as shown in the inset of Fig. 4. The different dependences of the switching fields on the sampling position for the ascent and descent branches indicate that the single domain wall motions are different for the two branches. The unique asymmetric magnetization reversal mechanism was verified by magneto-optical Kerr imaging.[40] The magnetization reversal process of the descent (ascent) branch was found to begin with the nucleation of reversed domains at the thick (thin) end, where the exchange anisotropy field was minimal (maximal) and the magnetostatic field was maximal (minimal). The asymmetry became more prominent for the thin FM layer.[16] Similar phenomena are expected in Py/CrAl bilayers with wedged FM layers.[17] The asymmetric mechanism may be different in various FM/AFM bilayers. For example, in NiO/Py bilayers, the ascent and descent branches are both accompanied by the nucleation and growth of reversed domains with different centre activities.[41] In MnF_2/Fe bilayers, however, the magnetization reversal process of two branches is accompanied by coherent rotation, and the nucleation and extension of reversed domains.[42]

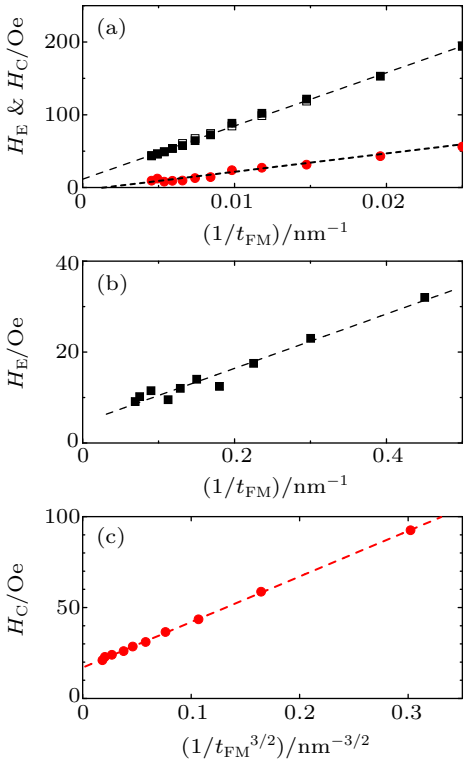


Fig. 3. (color online) Dependences of H_E (panels (a) and (b)) and H_C (panels (a) and (c)) at room temperature on t_{FM} for Py/FeMn panel (a) and Py/CrAl (panels (b) and (c)) bilayers. In panel (a) solid and open symbols correspond to measured data obtained by magnetometry and surface magneto-optical Kerr effect,[16,17] respectively.

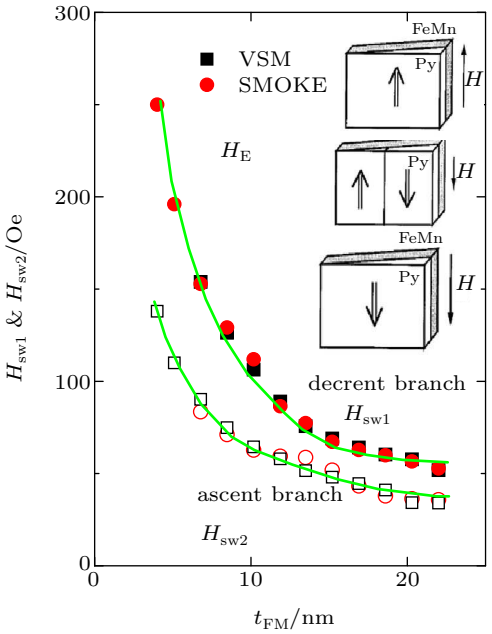


Fig. 4. (color online) Dependences of switching fields at room temperature of two branches on t_{FM} for wedged-Py/FeMn bilayers. Square and circle symbols correspond to measured data by magnetometry and surface magneto-optical Kerr effect,[16] respectively.

2.3. Effects of buffer layer thickness

Although fcc AFM Fe–Mn cannot exist in an equilibrium state below 500 K, metastable AFM fcc Fe–Mn films can often be obtained by magnetron sputtering or molecular beam epitaxial approaches. Previous experimental studies have shown that a preferred (111) orientation is required to establish the EB. The (111) atomic plane is both in-plane and out-of-plane spin-compensated. The microstructure of the metastable FeMn layer strongly depends on the deposition condition, the materials and thickness of the buffer layer. The effects of the buffer materials on the EB in Si(substrate)/buffer/NiFe/Cu/NiFe/FeMn spin valves have been studied by using various buffer materials including Nb, Ta, Ti, Zr, Hf, Cu, Ag, Au, and Cr.[43] Here, we study the effect of the Cu buffer layer thickness on the EB in substrate/wedged-Cu(0–30 nm)/FeMn(10.0 nm)/Py(25.0 nm) multilayers.[44] H_E at a specific temperature is found to increase approximately linearly with the increase of Cu buffer layer thickness as shown in the inset of Fig. 5(a). The room temperature H_C is also found to increase at a small Cu layer thickness and to approach a saturation at a thick Cu layer. For the Cu layer, thickness in a region from 0 to 30.0 nm, H_E is reduced as a linear function of T and vanishes at the blocking temperature T_B as shown in Fig. 5(a). In particular, the T_B sharply increases with an increasing Cu layer thickness and approaches to a constant at 15.0 nm as shown in Fig. 5(b). In general, the T dependence of the EB is thought to arise from the competition between the magnetic anisotropy of the AFM layer and the $\Delta\sigma$ at the FM/AFM interface. Since the T_B strongly depends on the thickness and microstructural properties of the AFM layer,[43,45,46] its increase with the increase of the Cu layer thickness can be attributed to the effect of the Cu layer thickness on either the improved fcc (111) texture or the enlarged grain size in the AFM FeMn layer.[43,45]

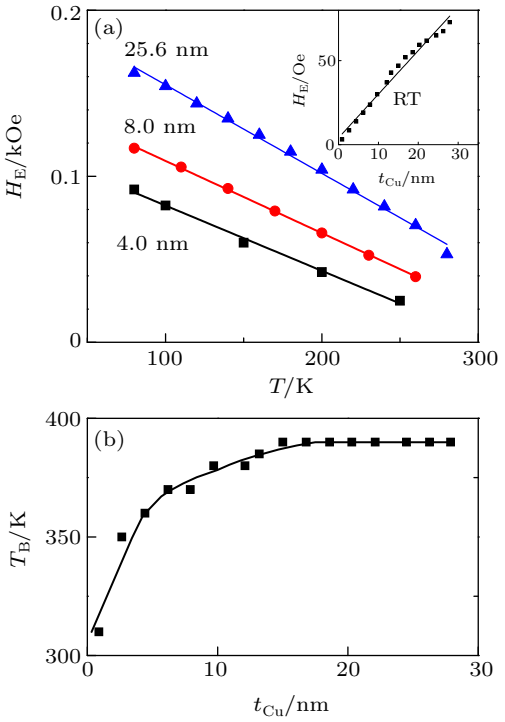


Fig. 5. (color online) Dependences of H_E on T (a) and dependence of T_B on Cu layer thickness (b) for substrate/Cu/FeMn/Py. In the inset the abscissa axis represents Cu layer thickness. The inset shows the dependence of H_E at room temperature on Cu layer thickness. Solid lines serve as a guide to the eye.[44]

2.4. Effects of microstructure in an FM layer

Although H_C of an FM/AFM bilayer is often enhanced in comparison with that of a single FM layer, it may be reduced for a particulate FM layer as discussed below. For Si substrate/Cu(30 nm)/$Co_{80}Cr_{20}$ (= CoCr)(0–30 nm)/FeMn (20 nm) multilayer,[47] a broad diffraction peak of CoCr ($10\bar{1}1$) was observed in an X-ray diffraction spectra. Moreover, α-FeMn (422) and γ-FeMn (111) diffraction peaks were also observed. Meanwhile, large samples of Fe_xCr_{1-x} (= FeCr) /$Ir_{0.25}Mn_{0.75}$ (= IrMn) bilayers with $t_{AFM} = 3$ nm and 6 nm were deposited on 1 cm × 5 cm glass substrates at ambient temperature.[48] Across the substrate length of 5 cm, x changes linearly from 0.34 to 0.51 as a function of the sampling location. As an ideal magnetic recording medium, in an equilibrium state the CoCr alloy with 20 at.% Cr consists of hexagonal closed packed Co-rich and tetragonal Cr-rich phases, as schematically shown in Fig. 6(a). At room temperature, the second phase is paramagnetic and is located between hexagonal closed packed Co-rich grains. Similarly, the Fe–Cr alloy also consists of the bcc Fe-rich and Cr-rich phase. The IrMn films deposited at ambient temperatures are of the fcc (111) structure. The inset in Fig. 6(b) shows that the EB is established in CoCr/FeMn bilayer and H_E changes as a linear function of $1/t_{FM}$, indicating the interfacial nature of the EB. In the CoCr/FeMn bilayer, the

$\Delta\sigma$ is as small as 0.011 erg/cm^2, and is much weaker than that of the Py/FeMn bilayer. H_C of both CoCr/FeMn bilayer and CoCr single layer film increase with the increasing of t_{FM}, as shown in Fig. 6(b). In particular, H_C of the CoCr/FeMn bilayer is smaller than that of the corresponding single layer film. The H_C reduction is also observed in the FeCr/IrMn bilayers with the Fe atomic concentration lower than 40 at.% as shown in Fig. 6(c). The unique phenomena can be attributed to two competing effects. On the one hand, the AFM layer has pinning effects on the magnetization reversal processes of the CoCr and FeCr layers due to the random field or interfacial magnetic frustration, leading to the H_C enhancement. On the other hand, the AFM layers provide additional interactions between the Co-rich and Fe–rich grains, in addition to the interaction through the paramagnetic Cr-rich components, leading to the H_C reduction. In short, as an extrinsic magnetic parameter, the unusual H_C behavior is attributed to the enhanced magnetic coupling between the Co(Fe)-rich grains due to the effect of the AFM layers.

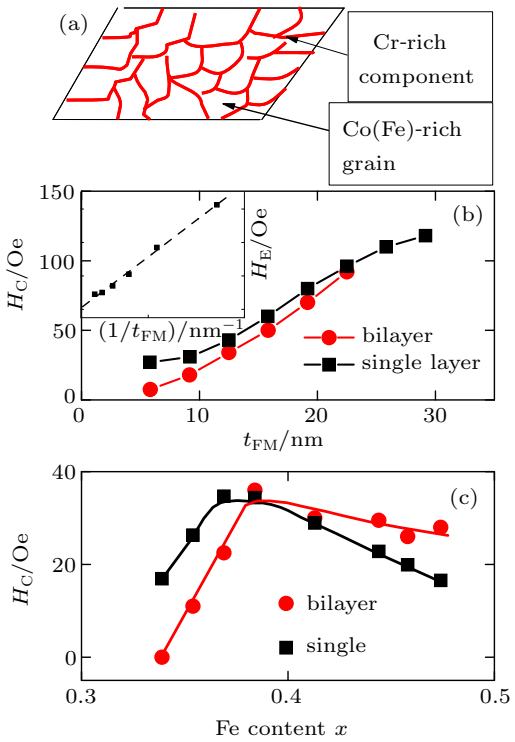


Fig. 6. (color online) Schematic diagram of the particulate structure in CoCr and FeCr layers (a), dependences of H_C on t_{FM} for CoCr/FeMn bilayers (b), and on Fe content in FeCr/IrMn bilayers (c). The inset in panel (b) shows the dependence of H_E on t_{FM}. For comparison, the data of FeCr single layer films is also given in panel (b). Measurements were performed at room temperature. Solid lines each serve as a guide to the eye.[47,48]

2.5. Effects of FM magnetization

For an FM/AFM bilayer, one has $H_E = \Delta\sigma/M_{FM}t_{FM}$, where $\Delta\sigma$ is the areal interfacial exchange interaction energy. Accordingly, one has $\Delta\sigma = \sum -2J_{ij}\boldsymbol{S}_{FMi}\cdot\boldsymbol{S}_{AFMj}$, where $\boldsymbol{S}_{FMi}$ and $\boldsymbol{S}_{AFMj}$ refer to the FM and AFM spins near the interface, respectively. If the areal density of the FM spins is n and each FM spin has m nearest-neighbouring AFM spins, then $\Delta\sigma = n\sum -2J_{1j}\boldsymbol{S}_{FM}\cdot\boldsymbol{S}_{AFMj}$ with $j = 1$ to m. Apparently, the magnitude of $\Delta\sigma$ at specific temperatures strongly depends on the magnitude and temperature dependence of the FM magnetization. Therefore, it is necessary to study the dependence of $\Delta\sigma$ on the FM magnetization. For this reason, several series of FM/AFM bilayers were prepared. A large specimen of $Co_{1-x}Ni_x$/FeMn (15 nm) was deposited onto a 30.0-nm Cu buffer layer to promote the growth of fcc (111) FeMn orientation.[49] The Co–Ni alloy layers were made by co-sputtering from Co and Ni targets such that there is a composition gradient varying from $x = 0.36$ to 0.94 across a length of about 10 cm. It is noted that the composition wedge in the FM layer can avoid the run-to-run error. The large sample was cut into twenty pieces of small specimens. The $\Delta\sigma$ can be obtained from the equation $\Delta\sigma = H_E M_{FM} t_{FM}$, with the data of H_E, the magnetic moments and the area of the specimen because the product of the FM magnetization and thickness of each sample is equal to the magnetic moment divided by the sample area. Another series of five substrate(Si)/Cu(30 nm)/FeMn(30 nm)/wedged-FM bilayers with FM = Ni, $Ni_{80}Fe_{20}$, $Ni_{50}Fe_{50}$, Co, and Fe were also fabricated, where these FM layers have different magnetizations.[50] Figure 7 shows that for all FM/FeMn bilayers with different FM layers, $\Delta\sigma$ at room temperature increases with the increasing of M_{FM} with a convex shape. It is found that the $\Delta\sigma$ of Fe/FeMn is about twice as much as that of Ni/FeMn bilayers, although the magnetization of Fe is about four times of that of Ni. For Co–Ni/FeMn bilayers, $\Delta\sigma$ increases by about 30% for M_{FM} from 600 (emu/cm^3) to 1200 (emu/cm^3). These results can be fitted by a linear $\sqrt{M_{FM}}$ dependence for Co–Ni/FeMn bilayers and the series of five samples. The effect of the FM magnetization on $\Delta\sigma$ can be further confirmed by the results for Fe–Cr/IrMn bilayers,[48] as shown in Fig. 7. Although the variation trends are close to each other for these three series, the difference is clearly seen. The data of a series of CoNi/FeMn samples and five FM/FeMn bilayers do not fall in a single curve. In particular, the $\Delta\sigma$ of FeCr/IrMn samples sharply increases with increasing M_{FM} at small value, in a way different from those of the other two series of samples. The observed inconsistency might be induced by the microstructural difference among these FM layers. The present results cannot be described by either the rigid model proposed by Meiklejohn and Bean or planar domain wall model proposed by Mauri *et al.*[1,2,5,51] In the first model, $\Delta\sigma$ is assumed to be proportional to the FM magnetization whereas in the second model, $\Delta\sigma$ is assumed to be independent of the FM magnetization because it is equal to the planar domain wall energy in the AFM layers, i.e. $2\pi\sqrt{A_{AFM}K_{AFM}}$, where A_{AFM} and K_{AFM} are the exchange and the uniaxial anisotropy constants in the AFM layers, respectively. This might stimulate further theoretical investiga-

tion. For instance, O'Grady *et al.*[52,53] have developed a new paradigm to determine the exchange coupling of the EB.

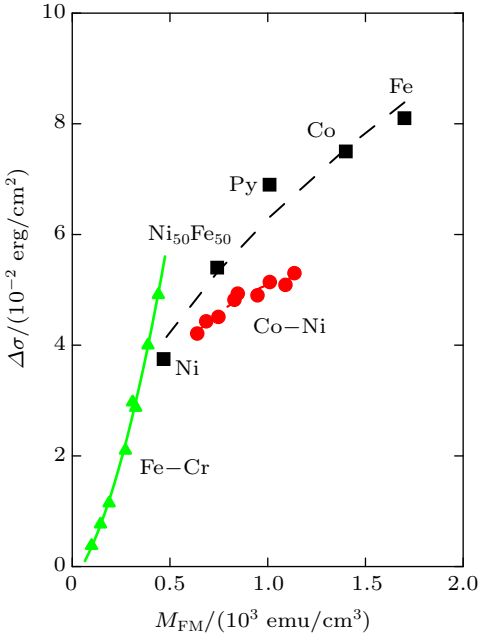


Fig. 7. (color online) Dependence of $\Delta\sigma$ at room temperature on the FM magnetization for FeCr/IrMn bilayers and FM/AFM bilayers with AFM = FeMn, FM = Ni, Py, $Ni_{50}Fe_{50}$, Co, and Fe.[48–50]

3. Positive EB

In conventional FM/AFM bilayers, the negative H_E is observed when the external magnetic field is parallel to the cooling magnetic field. In the FM/FeF_2 and FM/MnF_2 bilayers, however, a positive H_E can be obtained. Since the EB in the FM/AFM bilayer is established by both the symmetry breaking and small net magnetic moment of the AFM layer after the field cooling procedure, the positive EB is explained in terms of the interlayer antiferromagnetic coupling between the FM and AFM moments.[54,55] The positive EB has distinct features. The H_E changes its sign from positive to negative when the cooling magnetic field H_{CF} decreases. At the same time, the H_C acquires a maximal value near the crossover H_{CF}. Therefore, the EB is sensitive to H_{CF} magnitude whereas for a conventional FM/AFM bilayer with ferromagnetic coupling at the interface the EB is almost independent of H_{CF} magnitude if the FM layer is saturated.[56,57] Here, we study the positive EB in an FM/AFM bilayer by using GdFe = $Gd_{45}Fe_{55}$/NiCoO (= $Ni_{46}Co_{54}$) bilayer.[58] Here, NiCoO is a typcial AFM material and GdFe is a typical AFM alloy. T_N of NiCoO layer is about 400 K so that the field cooling procedure can be performed using the physics property measurement system. Atomic magnetic moments of Gd from spin and orbital angular momenta are parallel to each other whereas that of Fe is mainly contributed from the spin angular momentum due to the quenched orbital angular momentum. With antiferromagnetic coupling between the spins of Gd and Fe atoms, their atomic magnetic moments are antiparallel to each other. Accordingly, the net magnetization of the $Gd_{45}Fe_{55}$ alloy is parallel to that of the heavy rare-earth atoms because the Gd contribution is dominant. Due to antiferromagnetic coupling between the spins of Gd in the FM layer and the spins of Ni and Co in the AFM layer, the net magnetization of the FM layer is antiferromagnetically coupled to the net magnetic moment of the AFM layer. For the small H_{CF}, the FM magnetization and AFM magnetization are parallel and antiparallel to the H_{CF} during the field cooling procedure, respectively, as shown in Fig. 8(a). After field cooling, the AFM magnetization is still antiparallel to the H_{CF} and the FM magnetization is energetically favorable for being parallel to H_{CF}, leading to a negative H_E. At a high H_{CF}, the AFM and FM magnetizations are both parallel to H_{CF}. After field cooling, the AFM magnetization is still parallel to H_{CF} and the FM magnetization is energetically favorable to being antiparallel to H_{CF}, leading to a positive H_E, as shown in Fig. 8(b). The H_E increases from −6 Oe to 50 Oe when the H_{CF} increases from 0 to 15 kOe, with a crossover H_{CF} of about 200 Oe as shown in Fig. 8(c). The magnitude of the crossover cooling field directly reflects the antiferomagnetic coupling strength between FM and AFM spins. At the crossover H_{CF}, a multi-domain structure in the AFM layer is formed and then fixed after the field cooling procedure, and an additional pinning effect of the AFM domain walls on the motion of the FM domain wall occurs, leading to the H_C enhancement,[54] as shown in Fig. 8(d).

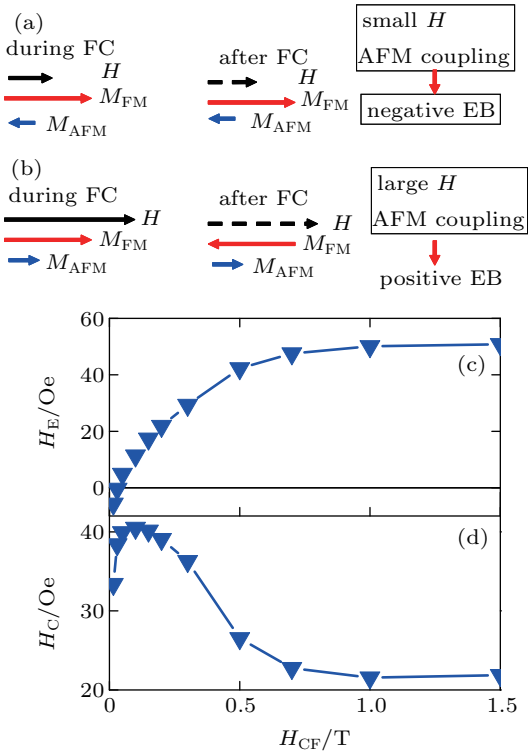


Fig. 8. (color online) Schematics for the mechanisms of negative (a) and positive (b) EB in FeGd/NiCoO bilayers. Dependences of H_E (c) and H_C (d) at 5 K on the cooling field.[58]

As a kind of magnetic anisotropy, it is significant to study the angular dependence of the EB (ADEB). The angular dependences of H_E and H_C were first studied in CoO/Py bi-

layers. H_E/H_C was found to be expressed by a $\cos(n\theta_H)$ series with $n =$ odd/even integral, where θ_H is the angle between the external magnetic field and the cooling field.[59] Since then, the ADEB has been studied in various FM/AFM bilayers and found to strongly depend on the physical properties of constituent layers, such as the canting of the interfacial spins and defects.[60] Figures 9(a) and 9(b) show the angular dependences of the room temperature EB in GdFe(15 nm)/FeMn(10 nm) bilayers with $H_{CF} = 300$ Oe and 15 kOe, respectively.[61] Clearly, H_E exhibits the unidirectional symmetry, i.e. $H_E(\theta_H) = H_E(-\theta_H)$ and $H_E(\theta_H) = -H_E(\theta_H \pm 180^\circ)$ whereas H_C shows the uniaxial symmetry, i.e. $H_C(\theta_H) = H_C(-\theta_H)$ and $H_C(\theta_H) = H_C(\theta_H \pm 180^\circ)$. In particular, the negative and positive EB have almost the same angular dependence, indicating the same magnetization reversal mechanism under different H_{CF}. Since H_E has a small valley in the vicinity of $\theta_H = 0$ and 180°, the angular dependence of the H_E cannot be described by a simple cosine function and high order terms must be considered. The calculations in Fig. 9(c) indicate that the small valley is induced by the uniaxial anisotropy in the GdFe layer and its depth strongly depends on the ratio H_C/H_E. In short, the present results in GdFe/NiCoO bilayers reproduce major features of the FeF_2/FM bilayers.[54]

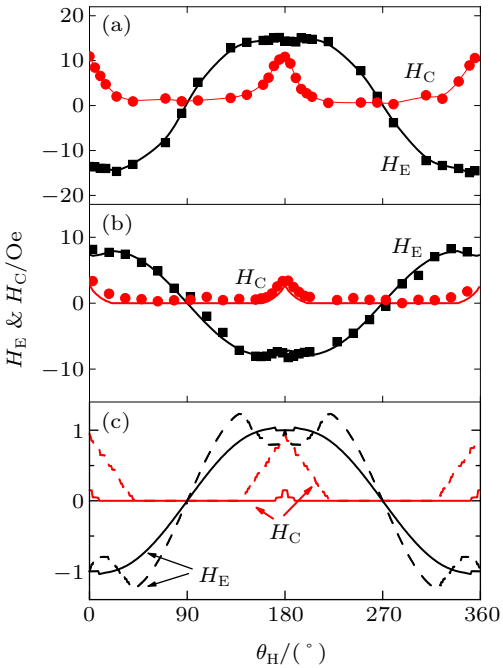


Fig. 9. (color online) Measured (panels (a) and (b)) and calculated (panel (c)) angular dependence of H_E and H_C (panels (a), (b), and (c)) at room temperature in FeGd/NiCoO bilayers. Solid lines in panels (a), (b), and (c) refer to fitted and calculated results,[61] respectively.

4. Perpendicular EB

Since the first observation of the perpendicular EB in $[Co/Pt]_n$/CoO multilayers,[62] the perpendicular EB has been studied extensively.[63–65] Here, Py/CoO multilayers were fabricated by DC magnetron sputtering and perpendicular EB was studied.[66] X-ray diffraction measurements show that both the Py and CoO layers are of fcc (111) texture. Figure 10 shows typical out-of-plane and in-plane hysteresis loops after the sample has been cooled from room temperature to a low temperature under a zero magnetic field and nonzero magnetic fields, perpendicular and parallel to the film plane. With the perpendicular cooling magnetic field, the out-of-plane hysteresis loops are shifted away from the zero magnetic field and the perpendicular EB is established. One has $H_E = -750$ Oe, 0, and -150 Oe with perpendicular and parallel cooling fields and zero cooling field,[67] respectively. In the in-plane hysteresis loops, one has $H_E = -1.4$ kOe, 0, and -1.42 kOe with in-plane and perpendicular cooling field and zero cooling field, respectively. The perpendicular magnetic anisotropy can be established even with the zero magnetic field cooling procedure, which might be related to the spin structure of a CoO layer. In each (111) atomic plane, all Co spins are parallel to each other but they are antiparallel to each other in neighbouring (111) planes. Since all Co spins are parallel to [117] axis,[68] they are located on cone surfaces with a half-apex angle of 66.2° for polycrystalline CoO layer, leading to a perpendicular magnetic moment component. The out-of-plane component of AFM spins was also found in a perpendicular exchange biased $[Co/Pt]_n$/IrMn multilayer by tunneling anisotropy magnetoresistance measurements.[69] It is shown that for the Py/CoO multilayer H_E can be fitted by a linear function of $1/t_{FM}$ and one has $\Delta\sigma = 0.12$ erg/cm^2 at 5 K, smaller than the value of 0.25 erg/cm^2 at 10 K for $[Co/Pt]_n$/CoO multilayer possibly due to a smaller magnetization of the Py layer in comparison with that of the Co layer.[62] Moreover, H_C can be fitted to a linear function of $(1/t_{FM})^{3/2}$, similar to the results of the longitudinal EB in Py/CoO bilayers, which can be explained in terms of the random field model.[37] In the experiment, the initial magnetization curves were measured with H in the film plane and along the film normal direction. The effective magnetic anisotropy was taken as the difference in the integration $\int H\mathrm{d}M$ between the directions. Figures 11(a) and 11(b) show that the term $K_{eff}t_{FM}$ decreases with increasing T in similar ways for various t_{FM}, indicating the interfacial nature of the effective anisotropy. The interface anisotropy constant K_S is calculated to be 0.4 erg/cm^2 at 5 K and approaches zero near the Neél temperature of CoO layer. Therefore this illustrates that the K_S is induced by the antiferromagnetic ordering of the CoO layer. In most studies, perpendicularly magnetized multilayers are often used as FM layers.[62–65] In contrast, the present Py layer with in-plane anisotropy is used as an FM layer and strong perpendicular anisotropy is introduced by the AFM CoO layer even under a zero field cooling procedure. The perpendicular EB has also been established in the Py/FeMn multilayer.[70] This

might provide a new clue to the realizing of the perpendicular magnetic anisotropy and will be helpful for the design and fabrication of new spintronics devices.

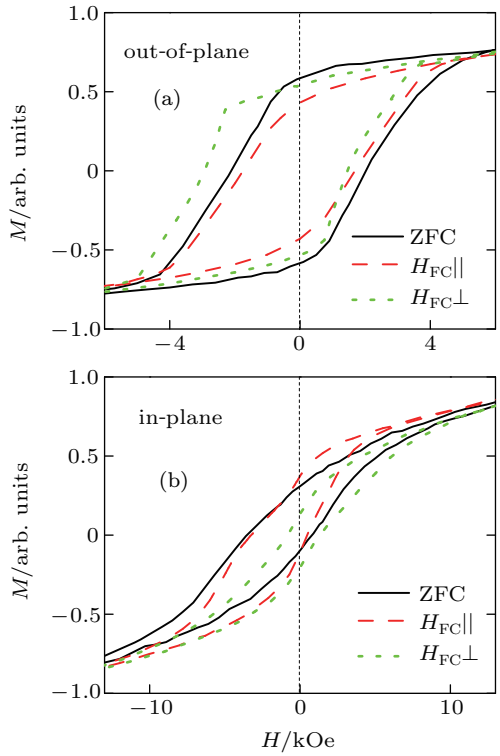


Fig. 10. (color online) Out-of-plane (a) and in-plane (b) hysteresis loops of [CoO (2.4 nm)/Py (2.0 nm)]$_{40}$ at 100 K with zero field cooling and 20 kOe cooling field parallel and perpendicular to the film plane.[67]

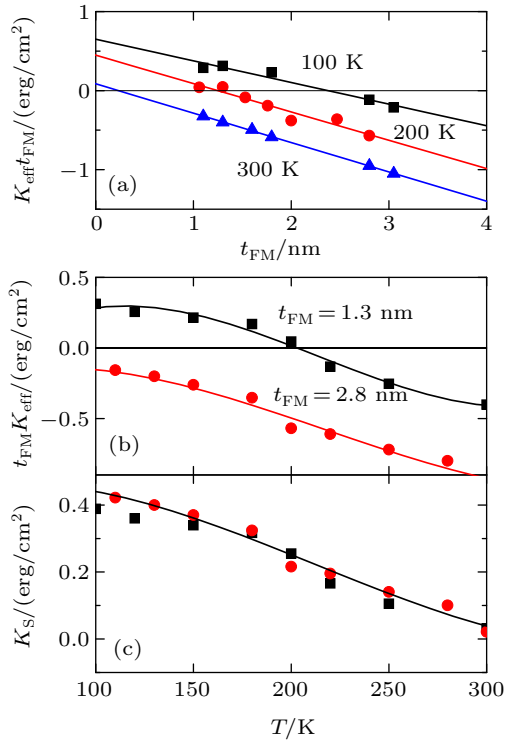


Fig. 11. (color online) Dependence of the effective magnetic anisotropy on the Py layer thickness at different temperatures (a) and on T at different t_{FM} (b). In panel (c) the induced interfacial magnetic anisotropy values fall onto the same curve after excluding FM thickness effects. The curves in panel (a) show linear fitted results.[66]

5. Hysteretic behavior of ADEB

For single FM layers, the torque curves measured in clockwise (CW) and counter clockwise (CCW) rotations normally overlap with each other for H larger than the saturation field, whereas for exchange-biased FM/AFM bilayers the rotational hysteresis loss still exists for H larger than the saturation field as a fingerprint of the EB.[1,5] It is indicated that the magnetization motion during the CW and CCW rotations is irreversible and can be attributed to the irreversible motion of AFM spins even for H larger than the saturation field. Similarly, during measurements of the angular dependence of hysteresis loops, the AFM spins are generally not saturated. In the case of the rigid model, the AFM spins are fixed for thick AFM layers. For Py/CoO bilayers with thick CoO layers, the angular dependence of the ADEB is identical for CW and CCW rotations.[59] For thin AFM layers, however, the irreversible motion of AFM spins may be involved during consequent CW and CCW rotations, and the hysteresis loops may be different at specific θ_H. The irreversible motion of AFM spins manifests itself as a hysteretic behavior of ADEB in CW and CCW rotations as discussed below.[71] In the present experiments, the angular-dependent hysteresis loops were measured with θ_H from -270° to 270° in CCW and from 270° to -270° in CW rotations for the polycrystalline Py/FeMn bilayers with thin AFM layers. With a vector magnetometry, the magnetization components m_x and m_y were measured which are parallel and perpendicular to the applied magnetic field, respectively. At a specific θ_H, H_E, H_C, m_{y-AVE}, and the asymmetry δ all depend on the CCW or CW rotation. Here, $m_{y-AVE} = m_{y-R} + m_{y-L}$ and the asymmetry $\delta = (\text{abs}(m_{y-R}) - \text{abs}(m_{y-L}))/(\text{abs}(m_{y-R}) + \text{abs}(m_{y-L}))$, where m_{y-R} and m_{y-L} are the values of m_y near the coercive fields. Figure 12 shows the hysteretic behaviors of the ADEB with CW and CCW rotations of θ_H from $\pm 90^\circ$ to $\mp 90^\circ$. Apparently, H_C has different angular dependences for CW and CCW rotations, peaking at $\theta_H = 20^\circ$ and -20°, respectively. Since H_E changes slowly and smoothly near 0° and 180°, the hysteretic behavior of the angular dependence of H_E is less prominent than that of H_C.

In order to further understand the physics behind the hysteretic behavior, the pinning direction (PD) is introduced and defined as the direction of the FM magnetization at the remnant state.[72] The PD orientation can be measured by the torque curves under zero H. When the PD is parallel to the H axis in the magnetometry system, m_x acquires a maximal value accompanied by zero m_y. The torque measurement is performed after each hysteresis loop during measurements of the ADEB. At first, the PD also exhibits a hysteretic behavior peaking at $\theta_H \approx 20^\circ$ and -20° during CW and CCW rotations, respectively,[73] as shown in Fig. 12(e). The θ_{PD} and H_C show correlated angular variation trends and acquire maximal

(minimal) values at the same θ_H during either CW or CCW rotation. The angular difference $\Delta\theta_{PD}$ between the maximal and minimal θ_{PD} values can be used to quantify the degree of the hysteretic behavior.

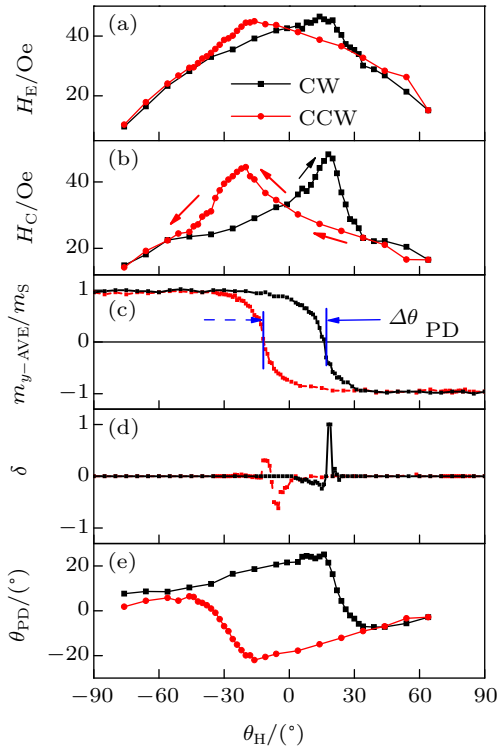


Fig. 12. (color online) Measured angular dependence of room temperature H_E (a), H_C (b), normalized m_{y-AVE}/m_s (c), asymmetric factor δ (d), and θ_{PD} (e) of Py/FeMn bilayer for CW and CCW rotations, where the m_s is the saturation magnetic moment.[71,73]

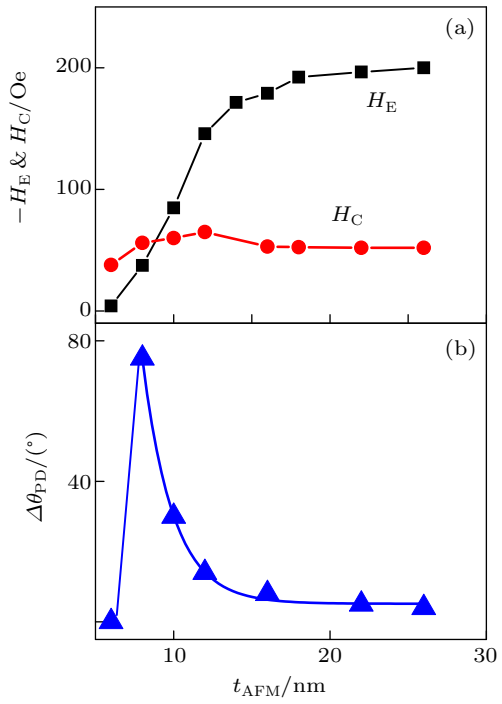


Fig. 13. (color online) Dependence of room temperature H_E and H_C (a), and $\Delta\theta_{PD}$ (b) in Py/FeMn bilayer on t_{AFM}.[71,73]

In the experiment, $\Delta\theta_{PD}$ is found to be independent of t_{FM} whereas it strongly depends on t_{AFM}.[71] It equals zero for very thin AFM layers and increases to a maximal value of about 70° with further increasing of t_{AFM} as shown in Fig. 13. For thicker AFM layers, the hysteretic behavior becomes weak and even disappears, which accords with the previous results that the ADEBs are almost identical for the CW and CCW senses.[57,74] More remarkably, the position of the maximal $\Delta\theta_{PD}$ is very close to that of the H_C, which are both located at the sharp variation of H_E. Moreover, the hysteretic effect depends on the AFM material. For example, the hysteretic behavior in the Co/IrMn bilayer is much weaker than that of the Py/FeMn bilayer, possibly due to the large uniaxial anisotropy constant of the IrMn material.[75] As a basic feature of the EB, the hysteretic behavior of the ADEB has also been observed in Co/FeMn, Co/IrMn, and Ni/NiO bilayers[75–78] and can be explained as a result of the irreversible motion of AFM spins.

6. EB training effect and rotatable anisotropy

For the FM/AFM bilayer, H_E and H_C often decrease during consecutive measurements of hysteresis loops. The EB training effect is an important phenomenon and has therefore been studied extensively.[72,79–86] Figure 14(a) shows consecutive hysteresis loops for Py/FeMn bilayers. The switching field of the descent branch decreases whereas that of the ascent branch remains virtually unchanged, demonstrating the type I training effect.[50,80] Both H_E and H_C are reduced with n as shown in Fig. 14(c). For a perpendicularly magnetized Pt(3 nm)/Co(0.5 nm)/Pt(0.5 nm)/IrMn(4 nm) multilayer, the perpendicular EB exhibits the type II training effect.[80,87] As shown in Fig. 14(b), during consecutive measurements, two branches of hysteresis loop are shifted at almost the same steps. For the cycle number n changing from 1 to 30, H_E is reduced by 50% whereas H_C almost does not change as shown in Fig. 14(d). The type II EB training effect has also been observed in Fe_xCr_{1-x}/IrMn with longitudinal geometry when the Fe content x was lower than 0.4.[48,80] For the Pt/Co/Pt/IrMn multilayers and FeCr/IrMn bilayers,[48,87] the m_y component is always zero during the FM magnetization reversal process. The coercivity increases with the increasing of θ_H, obeying a linear relationship $1/\cos(\theta_H)$ where $\theta_H =$ the angle between H and the film normal direction. Therefore, the magnetization reversal process is accompanied by the pinned domain wall motion for two branches in Pt/Co/Pt/IrMn bilayer. For Py/FeMn bilayer with uniform constituent layers, however, the magnetization reversal process is partly accompanied by coherent rotation of domains for two branches. Apparently, the EB training effect strongly depends on the magnetization reversal mechanism of the FM layers. Moreover, the EB training effect can also be tuned by recovery and torque approaches.[88,89] For both Py/FeMn bilayers and

Pt/Co/Pt/IrMn multilayers, H_E and H_C both decrease with the cycle number n and their variations can be described by the linear function of $1/\sqrt{n}$ except for $n = 1$ as shown in Figs. 14(c) & 14(d).[90,91] The $1/\sqrt{n}$ dependence can be explained in terms of a thermodynamic approach proposed by Binek.[82] The differences of H_E and H_C between $n = 1$ and $n = 2$ are attributed to the change in the asymmetric magnetization reversal process as an athermal effect.[92]

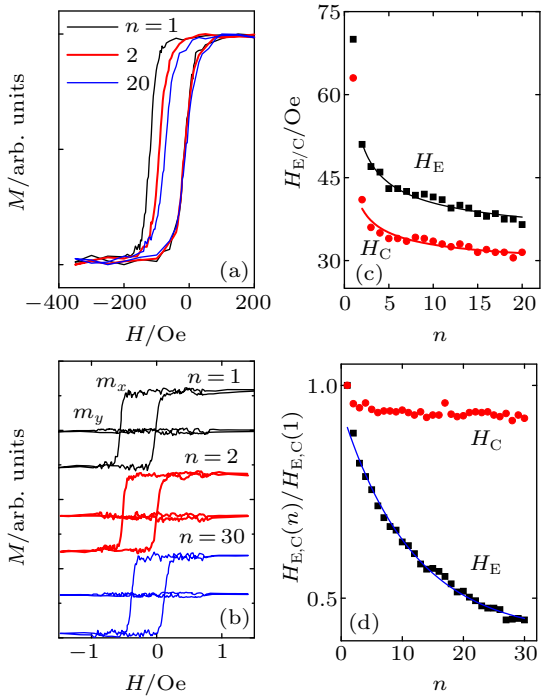


Fig. 14. (color online) Consecutive in-plane hysteresis loops for Py/FeMn bilayers (a) and out-of-plane ones for Pt/Co/Pt/IrMn multilayers (b). Dependence of H_E and H_C on the cycle number for Py/FeMn bilayers (c) and Pt/Co/Pt/IrMn multilayers (d).[71,87] The curves in panels (c) and (d) are linear fitted results of $1/\sqrt{n}$.

In order to reveal the physics behind the EB training effect, θ_{PD} is measured in a remnant state after each hysteresis loop during consecutive hysteresis loops at $\theta_H = -12°$. During the cycle training, the PD deviates from the initial PD direction and θ_{PD} changes from zero to 23°, in addition to the H_E and H_C reduction as shown in Figs. 15(a) and 15(b). More importantly, in addition to H_E and H_C, the θ_{PD} variation can also be fitted by the empirical law of $1/\sqrt{n}$ as shown in Figs. 15(c) and 15(d). At large n, the PD approaches to a fixed direction. The EB training effect can be attributed to two effects. At a specific θ_H, the H_E and H_C degradation are first related to the reductions of the unidirectional and the uniaxial anisotropic constants. Secondly, with the PD rotation, the angle between H and the transient easy axis increases as the cycle number n increases. The measuring H is accordingly deviated from the easy axis, leading to the reduced H_E and H_C. The PD rotation, therefore, also has an important impact on the EB training effect.

It is significant to study the dependence of the PD rotation on both the θ_H and t_{AFM}. Figures 16(a) and 16(b) show $\Delta H_{E/C}/H_{E/C}$ $(n = 1)$ and $\Delta\theta_{PD}$ in Py/FeMn bilayer each as a function of θ_H, where $\Delta H_{E/C} = H_E(1) - H_E(20)$ and $\Delta_{PD} = \theta_{PD}(20) - \theta_{PD}(1)$.[72] The θ_{PD} changes non-monotonically with θ_H whereas the $\Delta H_{E/C}/H_{E/C}$ $(n = 1)$ decreases monotonically. At $\theta_H = 0$, $\Delta\theta_{PD} = 0$ albeit a very large $H_{E/C}$ reduction.AQ1 Therefore, PD rotation does not occur in most studies of the EB training when the external magnetic field is generally parallel to the cooling field direction. At large negative θ_H, the PD rotation becomes smaller. At $\theta_H = -12°$, $\Delta\theta_{PD}$ acquires a maximal value. The EB training effect also depends on t_{AFM} as shown in Fig. 16(c). The EB training effect vanishes for small t_{AFM} and becomes maximal as H_E and H_C reduce of 60% and 40% at $t_{AFM} \approx 2.0$ nm, respectively. For a thicker AFM layer, it becomes weaker again. A large training effect is often observed for an ultra thin AFM layer or ultra-small AFM grains.[83,87] For an NiFe/CoO layer with an average AFM grain size of 4.0 nm, for example, H_E is reduced by 69% from $n = 1$ to 2.[83] Similar phenomena were also observed in a CoFe/IrMn bilayer.[93] More remarkably, a similar variation trend is observed for θ_{PD} as shown in Fig. 16(d). The maximal $\Delta\theta_{PD}$ is located at almost the same $t_{AFM} = 2.0$ nm for the maximal reductions of H_E and H_C.

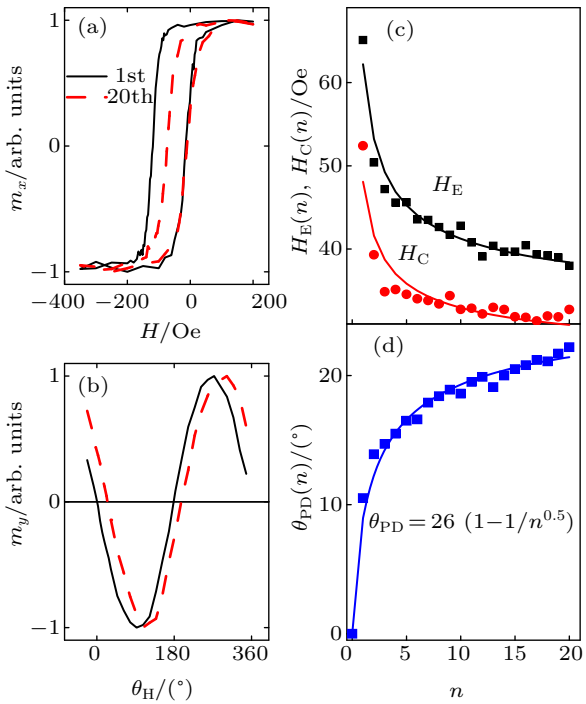


Fig. 15. (color online) Hysteresis lops (a) and torque curves at zero H (b) of consecutive cycles for Py/FeMn bilayers. Dependence of H_E and H_C (c) and θ_{PD} (d) on the cycle number. The curves in panels (c) and (d) are linear fitted results of $1/\sqrt{n}$.[72]

From the above analysis, the values of $\Delta\theta_{PD}$ for both the hysteretic behaviors of the ADEB and the EB training effect are correlated to the EB. Its training effect as a function of t_{AFM} are shown in Figs. 13 and 16. The strong correlation among these physical parameters can be explained in the frame of the theoretical models for polycrystalline FM/AFM

bilayers proposed in Refs. [94]–[97]. The AFM grains are assumed to be magnetically independent and are classified as rotatable or non-rotatable. The H_E is caused by AFM spins in non-rotatable AFM grains[95,96] whereas the H_C enhancement is caused by the irreversible rotation AFM spins in rotatable AFM grains. On the other hand, the possibility of the AFM spin rotation is governed by the competition between the thermal energy at finite T and the energy barrier of the AFM grains, i.e. the product of the uniaxial anisotropy and the grain volume.[94] Under the assumption of column structures in FM and AFM layers, the barrier height is proportional to the film thickness. For thin AFM layers, the AFM grain volume is very small and the thermal energy is larger than the barrier height, leading to the superparamagnetism of AFM spins at finite T. Neither the pinning effect nor irreversible rotation exists for AFM spins, leading to zero H_E and negligible H_C enhancement. At the same time, the hysteretic behavior of the ADEB and the EB training effect both disappear. For large t_{AFM}, the energy barrier height is larger than the thermal energy k_BT. Most of the AFM grains become thermally stable during the FM magnetization reversal process, leading to large H_E, small H_C, and a weak EB training effect. At intermediate t_{AFM}, the energy barrier is comparable to the k_BT, both rotatable and non-rotatable grains exist, leading to the maximal H_C and nonzero H_E. Meanwhile, the EB training effect becomes maximal.

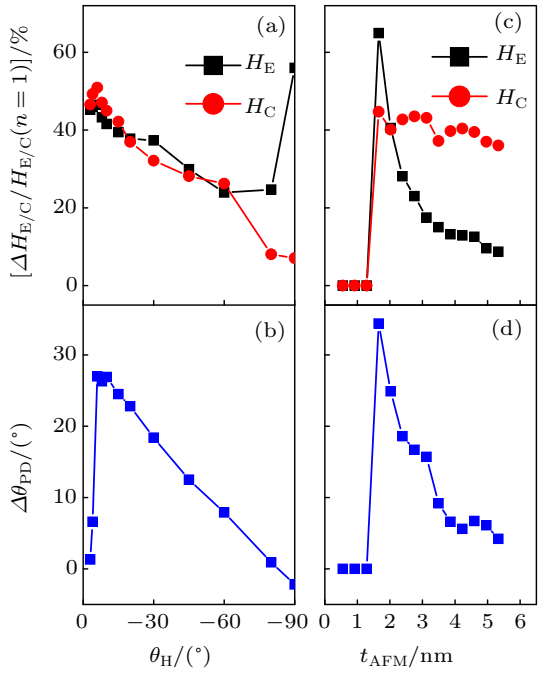


Fig. 16. (color online) Dependence of $\Delta H_{E/C}/H_{E/C}$ $(n=1)$ (panels (a) and (c)) and $\Delta\theta_{PD}$ (panels (b) and (d)) on θ_H (panels (a) and (b)) and t_{AFM} (panels (c) and (d)). In panels (a) and (b) $t_{AFM} = 2.4$ nm. In panels (c) and (d) $\theta_H = -12^\circ$.[72]

In the frame of the thermal fluctuation model, the PD rotation in the EB training effect and the hysteretic behavior of the ADEB can be ascribed to the interplay between the asymmetry of the magnetization reversal process and the irreversible rotation of AFM spins, with the possibility governed by the competition between the thermal energy and energy barrier. First, we address the PD rotation in the EB training effect. As schematically shown in Fig. 17, on the assumption that H makes a small negative angle with respect to the initial PD, the FM domains are partly rotated through θ_H, 90°, and $180^\circ + \theta_H$ during the FM magnetization reversal process for two branches. Accordingly, the AFM spins may be rotated in the same channel. On average, the AFM spins will be located at a new equilibrium angular position after each hysteresis loop due to the asymmetric magnetization reversal process, and the PD will be rotated in the consecutive hysteresis loops. For $\theta_H = 0$ or close to 90°, the asymmetry becomes less prominent, the difference $\theta_{PD}(n+1) - \theta_{PD}(n)$ and $\Delta\theta_{PD}$ both decrease. For the maximal asymmetry at the intermediate θ_H, $\Delta\theta_{PD}$ reaches a maximal value. The irreversible rotation of the AFM spins acquires the highest possibility, resulting in the largest $\Delta\theta_{PD}$ for the intermediate t_{AFM}. At large and small t_{AFM}, the possibility of the irreversible rotation is very much suppressed and equals zero, leading to negligible $\Delta\theta_{PD}$. Therefore, the t_{AFM} dependence of $\Delta\theta_{PD}$ in the EB training effect can be easily understood. Secondly, the PD rotation in the hysteretic effect of the ADEB can be understood in a similar way. During the CCW rotation of ADEB measurements, the PD is rotated away from the cooling field direction towards a positive angle with an initial small negative θ_H. With the increasing of θ_H, the PD approaches to a final direction. When the θ_H is larger than the PD final direction, the PD is rotated back towards the initial direction, leading to the hysteretic behavior. In short, we have indirectly revealed the rotatable anisotropy in both the EB training effect and hysteretic behavior of the ADEB, which manifests itself as the PD rotation. Recently, rotatable and frozen AFM spins in Fe/CoO bilayers have been probed directly by X-ray magnetic circular dichroism and X-ray magnetic linear dichroism (XMLD) techniques.[98]

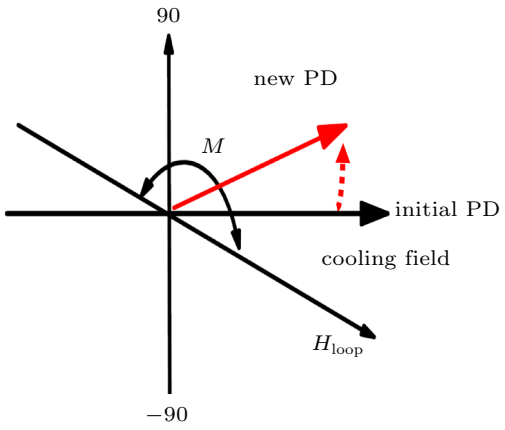


Fig. 17. (color online) Schematic diagram of FM magnetization and external magnetic field with respect to the cooling field direction for the PD rotation in the EB training effect and hysteretic behavior of the ADEB.

7. Summary

In this work, we have reviewed our investigations on the EB in FM/AFM bilayers. In the second part, we have addressed the effects of constituent layer thickness in Py/FeMn and Py/CrAl bilayers. H_E can be fitted as a linear function of $1/t_{FM}$ indicating the interfacial nature of the EB. The interfacial exchange coupling energy $\Delta\sigma$ in a Py/FeMn bilayer is larger than that of a Py/CrAl bilayer. H_E is found to change non-monotonically as a function of t_{AFM}. The onset thickness of CrAl layers is about one order larger than that of the FeMn layer. In a Cu/FeMn/Py system, H_E is found to increase with the increasing of Cu buffer layer thickness. Meanwhile, the $\Delta\sigma$ is found to be proportional to $\sqrt{M_{FM}}$ in Co–Ni/FeMn and FM/FeMn bilayers with FM = Ni, Ni–Fe, Co, and Fe. Moreover, the H_C reduction is found in CoCr/FeMn and FeCr/IrMn bilayers with particulate FM layers. In the third part, we have outlined the establishment of the positive EB in GdFe/NiCoO bilayers with antiferromagnetic coupling between FM and AFM magnetic moments. In the fourth part, we have described the establishment of the perpendicular EB in Py/CoO multilayers. The strong interface anisotropy is introduced by the CoO layers. In the last two parts, we have unveiled the mechanisms of both the hysteretic behavior of the ADEB and the EB training effect. In particular, we have revealed the role of the rotatable anisotropy in the two phenomena.

Acknowledgment

One of authors (Zhou Shi-Ming) would like to thank Prof. C. L. Chien in JHU and Prof. R. Chantrell in the University of York, and former students in our group including S. J. Yuan, L. Wang, R. Shan, T. R. Gao, D. Z. Yang, and X. P. Qiu for their great contributions to the above work.

References

[1] Meiklejohn W H and Bean C P 1956 *Phys. Rev.* **105** 904
[2] Meiklejohn W H 1958 *J. Appl. Phys.* **29** 454
[3] Kouvel J S and Graham Jr C D 1959 *J. Phys. Chem. Solids* **11** 220
[4] Kouvel J S 1959 *J. Appl. Phys.* **30** S313
[5] Meiklejohn W H 1962 *J. Appl. Phys.* **33** 1328
[6] Bean C P 1959 *Structure and Properties of Thin Films* (New York: John Wiley & Sons, Inc.) p. 331
[7] Baibich M N, Broto J M, Fert A, Nguyen Van Dau F, Petroff F, Etienne P, Creuzet G and Friederich A 1988 *Phys. Rev. Lett.* **61** 2472
[8] Dieny B, Speriosu V S, Parkin S S P, Gurney B A, Wilhoit D R and Mauri D 1991 *Phys. Rev. B* **43** 1297
[9] Nogués J and Schuller I K 1999 *J. Magn. Magn. Mater.* **192** 203
[10] Berkowitz A E and Takano K 1999 *J. Magn. Magn. Mater.* **200** 552
[11] Zhao H W, Lu M, Sui Y X, Zhai H R, Feng D, Chen Y, Dong G S and Jin X F 1997 *Appl. Phys. Lett.* **70** 2906
[12] Liu W, Liu X H, Cui W B, Gong W J and Zhang Z D 2013 *Chin. Phys. B* **22** 027104
[13] Wu X W and Chien C L 1998 *Phys. Rev. Lett.* **81** 2795
[14] Cai J W, Liu K and Chien C L 1999 *Phys. Rev. B* **60** 72
[15] Li H Y, Chen L Y and Zhou S M 2002 *J. Appl. Phys.* **91** 2243
[16] Zhou S M, Liu K and Chien C L 1998 *Phys. Rev. B* **58** 14717
[17] Zhou S M, Liu K and Chien C L 2000 *J. Appl. Phys.* **87** 6659
[18] Kouvel J S and Kasper J S 1963 *J. Phys. Chem. Solids* **24** 529
[19] Spišák D and Hafner J 2000 *Phys. Rev. B* **61** 11569
[20] Ishikawa Y and Endoh Y 1968 *J. Appl. Phys.* **39** 1318
[21] Lyman T 1973 *Metallography, Structures and Phase Diagrams*, Vol. 8, *Metals Handbook*, 8th edn. (Ohio: Metals Park) p. 287
[22] Fawcett E, Alberts H L, Galkin V Y, Noakes D R and Yakhmi J V 1994 *Rev. Mod. Phys.* **66** 25
[23] Mauri D, Kay E, Scholl D and Howard J K 1987 *J. Appl. Phys.* **62** 2929
[24] Jungblut R, Coehoorn R, Johnson M T, de Stegge J and Reinders A 1994 *J. Appl. Phys.* **75** 6659
[25] Gruyters M and Riegel D 2000 *Phys. Rev. B* **63** 052401
[26] Speriosu V S, Parkin S S P and Wilts C H 1987 *IEEE Trans. Magn.* **23** 2999
[27] Malozemff A P 1987 *Phys. Rev. B* **35** 3679
[28] Hu Y, Wu G Z, Liu Y and Du A 2012 *J. Magn. Magn. Mater.* **324** 3204
[29] Ali M, Marrows C H and Hickey B J 2003 *Phys. Rev. B* **67** 172405
[30] Allegranza O and Chen M M 1993 *J. Appl. Phys.* **73** 6218
[31] Lin T, Tsang C, Fontanat R E and Howard J K 1995 *IEEE Trans. Magn.* **31** 2585
[32] Gao T R, Shi Z, Zhou S M, Chantrell R, Asselin P, Bai X J, Du J and Zhang Z Z 2009 *J. Appl. Phys.* **105** 053913
[33] Sang H, Du Y W and Chien C L 1999 *J. Appl. Phys.* **85** 4931
[34] Hu J G, Jin G J and Ma Y Q 2003 *J. Appl. Phys.* **94** 2529
[35] Nowak U, Usadel K D, Keller J, Miltényi P, Beschoten B and Güntherodt G 2002 *Phys. Rev. B* **66** 014430
[36] Akbar S, Kakehashi Y and Kimura N 1998 *J. Phys.: Condens. Matter* **10** 2081
[37] Zhang S, Dimitrov D V, Hadjipanayis G C, Cai J W and Chien C L 1999 *J. Magn. Magn. Mater.* **198–199** 468
[38] Malozemoff A P 1988 *J. Appl. Phys.* **63** 3876
[39] Camarero J, Sort J, Hoffmann A, García-Martín J M, Dieny B, Miranda R and Nogués J 2005 *Phys. Rev. Lett.* **95** 057204
[40] Nikitenko V I, Gornakov V S, Shapiro A J, Shull R D, Liu K, Zhou S M and Chien C L 2000 *Phys. Rev. Lett.* **84** 765
[41] Nikitenko V I, Gornakov V S, Dedukh L M, Kabanov Y P, Khapikov A F, Shapiro A J, Shull R D, Chaiken A and Michel R P 1998 *Phys. Rev. B* **57** 8111
[42] Leighton C, Fitzsimmons M R, Yashar P, Hoffmann A, Nogués J, Dura J, Majkrzak C F and Schuller I K 2001 *Phys. Rev. Lett.* **86** 4394
[43] Nakatani R, Hoshino K, Noguchi S and Sugita Y 1994 *Jpn J. Appl. Phys.* **33**(1A) 133
[44] Li H Y, Li J, Yuan S J, Wang L, Zhou S M and Song J T 2002 *J. Magn. Magn. Mater.* **246** 1
[45] Choe G and Gupta S 1997 *Appl. Phys. Lett.* **70** 1766
[46] Ambrose T and Chien C L 1996 *Phys. Rev. Lett.* **76** 1743
[47] Shan R, Lin W W, Yin L F, Tian C S, Sang H, Sun L and Zhou S M 2005 *Phys. Rev. B* **71** 064402
[48] Shi Z, Qiu X P, Zhu J T, Chantrell R W, Mangin S and Zhou S M 2011 *Eur. Phys. J. B* **84** 173
[49] Zhou S M and Chien C L 2001 *Phys. Rev. B* **63** 104406
[50] Yuan S J, Wang L, Zhou S M, Lu M, Du J and Hu A 2002 *Appl. Phys. Lett.* **81** 3428
[51] Mauri D, Siegmann H C, Bagus P S and Kay E 1987 *J. Appl. Phys.* **62** 3047
[52] Vallejo-Fernandez G, Fernandez-Outon L E and O'Grady K 2007 *Appl. Phys. Lett.* **91** 212503
[53] O'Grady K, Fernandez-Outon L E and Vallejo-Fernandez G 2009 *J. Magn. Magn. Mater.* **322** 883
[54] Leighton C, Nogués J, Jönsson-Åkerman B J and Schuller I K 2000 *Phys. Rev. Lett.* **84** 3466
[55] Deng D S, Jin X F and Tao R B 2002 *Phys. Rev. B* **65** 1724022
[56] Moran T J and Schuller I K 1996 *J. Appl. Phys.* **79** 5109
[57] Ambrose T and Chien C L 1998 *J. Appl. Phys.* **83** 7222
[58] Yang D Z, Du J, Sun L, Wu X S, Zhang X X and Zhou S M 2005 *Phys. Rev. B* **71** 144417
[59] Ambrose T, Sommer R L and Chien C L 1997 *Phys. Rev. B* **56** 83
[60] Kim J V, Stamps R L, McGrath B V and Camley R E 2000 *Phys. Rev. B* **61** 8888
[61] Du J, Yang D Z, Bai X J, Wu X S, Hu A, Zhou S M and Sun L 2006 *J. Appl. Phys.* **99** 08C103
[62] Maat S, Takano K, Parkin S S P and Fullerton E E 2001 *Phys. Rev. Lett.* **87** 087202
[63] Liu Z Y and Adenwalla S 2003 *Phys. Rev. Lett.* **91** 037207

[64] Zhai Z H, Teng J, Li B H, Wang L J, Yu G H and Zhu F W 2006 *Acta Phys. Sin.* **55** 2064 (in Chinese)
[65] Gong W J, Liu W, Liu X H, Guo S, Feng J N, Li B and Zhang Z D 2011 *J. Appl. Phys.* **109** 043906
[66] Zhou S M, Sun L, Searson P C and Chien C L 2004 *Phys. Rev. B* **69** 024408
[67] Zhou S M, Yuan S J and Sun L 2005 *J. Magn. Magn. Mater.* **286** 211
[68] Roth W L 1958 *Phys. Rev.* **110** 1333
[69] Wang Y Y, Song C, Cui B, Wang G Y, Zeng F and Pan F 2012 *Phys. Rev. Lett.* **109** 137201
[70] Sun L, Zhou S M, Searson P C and Chien C L 2003 *J. Appl. Phys.* **93** 6841
[71] Gao T R, Yang D Z, Zhou S M, Chantrell R, Asselin P, Du J and Wu X S 2007 *Phys. Rev. Lett.* **99** 057201
[72] Qiu X P, Yang D Z, Zhou S M, Chantrell R, O'Grady K, Nowak U, Du J, Bai X J and Sun L 2008 *Phys. Rev. Lett.* **101** 147207
[73] Qiu X P, Shi Z, Zhou S M, Du J, Bai X J, Chantrell R and Sun L 2009 *J. Appl. Phys.* **106** 063903
[74] Xi H W, Kryder M H and White R M 1999 *Appl. Phys. Lett.* **74** 2687
[75] Zhang J, Du J, Bai X J, You B, Zhang W and Hu A 2009 *Chin. Phys. Lett.* **26** 047501
[76] Lommel J M and Graham C D 1962 *J. Appl. Phys.* **33** 1160
[77] Olamit J and Liu K 2007 *J. Appl. Phys.* **101** 09E508
[78] Yang P Y, Song C, Fan B, Zeng F and Pan F 2009 *J. Appl. Phys.* **106** 013902
[79] Schlenker C and Paccard D 1967 *J. Phys.* **28** 611
[80] Zhang K, Zhao T and Fujiwara H 2001 *J. Appl. Phys.* **89** 6910
[81] Hochstrat A, Binek C and Kleeman W 2002 *Phys. Rev. B* **66** 092409
[82] Binek C 2004 *Phys. Rev. B* **70** 014421
[83] Pina E, Prados C and Hernando A 2004 *Phys. Rev. B* **69** 052402
[84] Binek C, Polisetty S, He X and Berger A 2006 *Phys. Rev. Lett.* **96** 067201
[85] Hauet T, Borchers J A, Mangin P, Henry Y and Mangin S 2006 *Phys. Rev. Lett.* **96** 067207
[86] Xu M, Pan J, Shen Y and Hu J G 2010 *Acta Phys. Sin.* **59** 7357 (in Chinese)
[87] Shi Z, Qiu X P, Zhou S M, Bai X J and Du J 2008 *Appl. Phys. Lett.* **93** 222504
[88] Yang P Y, Song C, Zeng F and Pan F 2008 *Appl. Phys. Lett.* **92** 243113
[89] Shi Z, Du J, Chantrell R W, Mangin S and Zhou S M 2011 *Appl. Phys. Lett.* **98** 122507
[90] Paccard D, Schlenker C, Massenet O, Montmory R and Yelon A 1966 *Phys. Status Solidi* **16** 301
[91] Chan M K, Parker J S, Crowell P A and Leighton C 2008 *Phys. Rev. B* **77** 014420
[92] Hoffmann A 2004 *Phys. Rev. Lett.* **93** 097203
[93] Kim D Y, Yoon S S, Kim C G, Tsunoda M and Takahashi M 2009 *IEEE Trans. Magn.* **45** 3865
[94] Fulcomer E and Charap S H 1972 *J. Appl. Phys.* **43** 4190
[95] Stiles M D and McMichael R D 1999 *Phys. Rev. B* **59** 3722
[96] Geshev J, Pereira L G and Schmidt J E 2002 *Phys. Rev. B* **66** 134432
[97] Choo D, Chantrell R W, Lamberton R, Johnston A and O'Grady K 2007 *J. Appl. Phys.* **101** 09E521
[98] Wu J, Park J S, Kim W, Arenholz E, Liberati M, Scholl A, Wu Y Z, Hwang C Y and Qiu Z Q 2010 *Phys. Rev. Lett.* **104** 217204